PASJ: Publ. Astron. Soc. Japan , 1–??,
© 2009. Astronomical Society of Japan.

Evidence from EIS for axial filament rotation before a large flare

David R. Williams *, Louise K. Harra
Mullard Space Science Laboratory, UCL, Holmbury St Mary, Surrey, RH5 6NT, United Kingdom
drw@mssl.ucl.ac.uk
David H. Brooks *
Space Science Division, Naval Research Laboratory, Washington, DC 20375
dhbrooks@ssd5.nrl.navy.mil
Shinsuke Imada
National Astronomical Observatory of Japan, National Institutes of Natural Sciences, Mitaka, Tokyo, 181-8588, Japan
shinsuke.imada@nao.ac.jp
and
Viggo H. Hansteen
Institute of Theoretical Astrophysics, University of Oslo, PB 1029 Blindern, 0315 Oslo, Norway
viggo.hansteen@astro.uio.no

(Received 2009 January 19; accepted 2007 January 1)

Abstract

In this article, we present observations made with the Extreme-ultraviolet Imaging Spectrometer (EIS) on-board the *Hinode* solar satellite, of an active region filament in the He II emission line at 256.32 Å. The host active region (AR 10930) produces an X-class flare during these observations. We measure Doppler shifts with apparent velocities of up to 20 km s^{-1}, which are antisymmetric about the filament length and occur several minutes before the flare's impulsive phase. This is indicative of a rotation of the filament, which is in turn consistent with expansion of a twisted flux rope due to the MHD helical kink instability. This is the first time that such an observation has been possible in this transition-region line, and we note that the signature observed occurs before the first indications of pre-flare activity in the GOES solar soft X-ray flux, suggesting that the filament begins to destabilise in tandem with a reorganistation of the local magnetic field. We suggest that this expansion is triggered by the decrease of magnetic tension around, and/or total pressure above, the filament.

Key words: Sun: activity — Sun: filaments — Sun: transition region

1. Introduction

It has long been suspected that solar filaments are helical in structure (e.g., Rust & Kumar 1994), and much progress has been made in modelling both filaments (e.g., Amari et al. 1999) and filament eruptions using flux rope models in first two (Chen & Shibata 2000), then three dimensions (Amari & Luciani 1999; Török & Kliem 2005). Discussion of the drivers and triggers of solar eruptive events (non-compact flares, filament eruptions, coronal mass ejections) has sometimes necessarily led in recent years to a separation of the various observable aspects of these phenomena, and of their modelling, with a view to understanding the potential series of physical processes involved.

Theoretical modelling by Török & Kliem (2005), and comparison between these models and observations by Williams et al. (2005), indicated that the initiation of such eruptive events may happen well before observed flaring signatures. Although the latter work was unable to draw direct conclusions as to the initiation mechanism, the authors were able to strongly favour an MHD instability as the *driver* of the eruption, successfully isolating the latter from the question of the eruption trigger.

Williams et al. (2005) used *TRACE* (Handy et al. 1999) observations to demonstrate quantitative agreement between the morphology and velocity of an erupting filament, and that of an MHD instability. However, they were unable to show the filament's initial transition into non-equilibrium before the flare began. This was largely due to the nature of the observations: the emission from the erupting structure in the 1600 Å channel was dominated by the C IV resonance line doublet, normally only visible during flares. In this article, we present indications of pre-flare activity along a dark filament seen in He II (256.32 Å), in advance of signatures of flare activity seen in soft X-rays.

2. Observations & Method

2.1. Observations

The Extreme-ultraviolet Imaging Spectrometer (EIS; Culhane et al. 2007) on the *Hinode* satellite observatory (Kosugi et al. 2007) is a slit spectrometer, with a tilting mirror to allow the position of the Sun which is imaged

* Present Address: Hinode Team Office, ISAS/JAXA, 3-1-1 Yoshinodai, Sagamihara, Kanagawa, 229-8510, Japan

to change, in the direction perpendicular to the slit (and parallel to the dispersion direction). A three-dimensional dataset can be built up by scanning the slit across an area of Sun, creating an image out of neighbouring slit images, with spectral information at each pixel. This "rastering" process is often seen as a limitation, since a single snapshot of a region cannot be made in this way. However, since time information is encoded in the raster, this allows us to pick out times of interest based on the positions which show relevant signatures.

The data analysed here are taken from an *Hinode*/EIS raster scanning in steps of 1″ from solar west to east, over an area of 512″ × 256″ around active region 10930 on 2006-Dec-13. Exposures of 30 s at each position were used to build up a high-sensitivity spectrum in the chosen spectral windows. The raster lasted from 01:12 to 05:41 UT, and the resulting field of view comfortably covered the active region, as well as a large area of plage and quiet Sun to its east. During the scan, EIS's slit passed over a portion of this active region in which an X3.4 flare was taking place. Prior to this, the slit passed over a filament which extended more than 100″ westward from the area of flare activity subsequently captured.

2.2. Analysis Method

The EIS data we use contain many spectral windows, but here we analyse a spectral window of width 0.53 Å around the He II line at 256.32 Å (the hydrogen-like Lyβ transition, $3p \rightarrow 1s$). To analyse the velocity behaviour in this active region, we fit a single Gaussian profile to the emission line with a linear background, using a Levenberg-Marquardt least-squares minimisation algorithm; this fit is performed for each spatial pixel in the raster. Note that we also fit a double-Gaussian model, also with background, but find that it makes no appreciable difference to the findings described below. As a control check, we also perform the same analysis on a similar spectral range around the strong Fe XII line at 195.12 Å.

The determination of the rest wavelength of the emission line is complicated by an orbital variation in the line position. However, this can be adequately subtracted by taking an average over a portion of the slit which rasters over only quiescent Sun. The rest of the calibration is performed using the preparation software suite available in the free SolarSoft IDL library (Freeland & Handy 1998).

In Figure 1, we present the fitted shift of the line centroid from the mean rest wavelength (Fig. 1a) and line-integrated intensity (Fig. 1b) in an area 256″ square around the active region. In order to illustrate the behaviour of the filament before the flare, we concentrate on an area 60″ square where substantial velocity shifts can be seen in two regions parallel to the filament. The white crosses in Figure 1c indicate positions where the line-of-sight velocity reaches almost zero; ($\|v\| < 2$ km s^{-1}), as determined by vertical slices through the filament. Three such slices are shown by solid white lines. These "negligible-velocity" positions are reproduced on the (logarithmic) line-intensity map in Figure 1d, and are seen to lie along the filament itself. Since the intensity minima

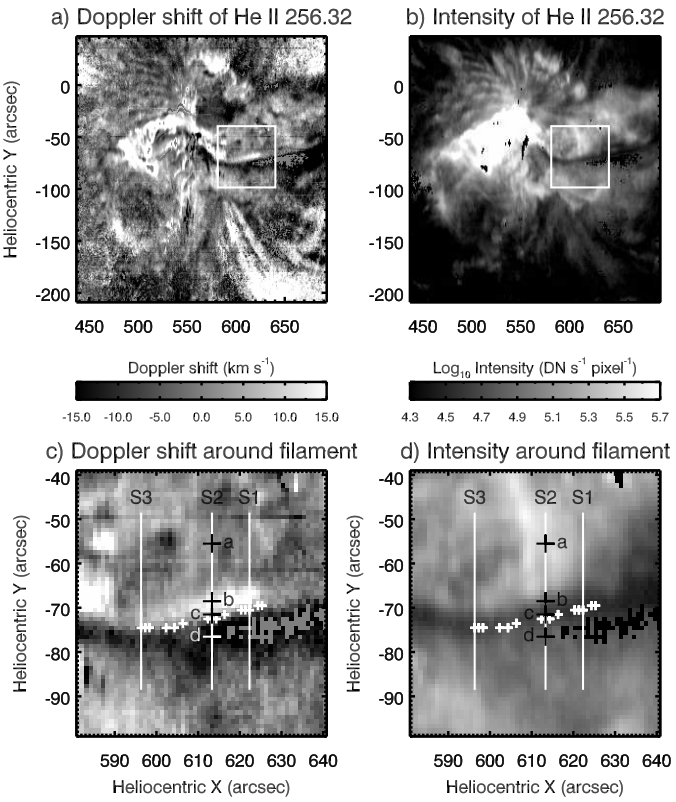

Fig. 1. (a) Plot of the fitted line-centre shift of He II λ256.32, with velocity-shift scale below. (b) Fitted line-integrated intensity of the same line, with logarithmic intensity scale below. (c) Magnification of area within white box in (a). Positions where the fit is bad are obvious, appearing as either grey pixels in velocity images, or black pixels in intensity images. The small white crosses in panels (c) and (d) indicate positions along the filament where the measured Doppler shift is negligible. The result of slicing through the close-up regions along vertical lines S1 to S3 is shown in Figure 2. Labelled crosses show the positions at which the line profiles in Figure 3 were taken (labels correspond to panels in the latter figure). We adopt the convention that negative velocity indicates blue-shifted emission.

are difficult to pick out by eye, the values of intensity and velocity along slices $S1$ to $S3$ are plotted in Figures 2a to 2c, respectively.

3. Discussion

3.1. Observed characteristics

He II λ256.32 is an optically thick line; for a coarse estimate of the line opacity, we follow Jordan (1967) to derive an opacity of order $\tau \approx 10^4$ at line centre, assuming a path length equivalent to the observed horizontal prominence width (8×10^8 cm), an electron density $n_e = 10^{10}$ cm^{-3}, and an electron temperature $T_e = 5 \times 10^4$ K. Since the detected intensity will approximately be formed where the optical depth is unity – if we employ the Eddington-Barbier approximation – we therefore assume that the line emission from the dense filament is dominated by emis-

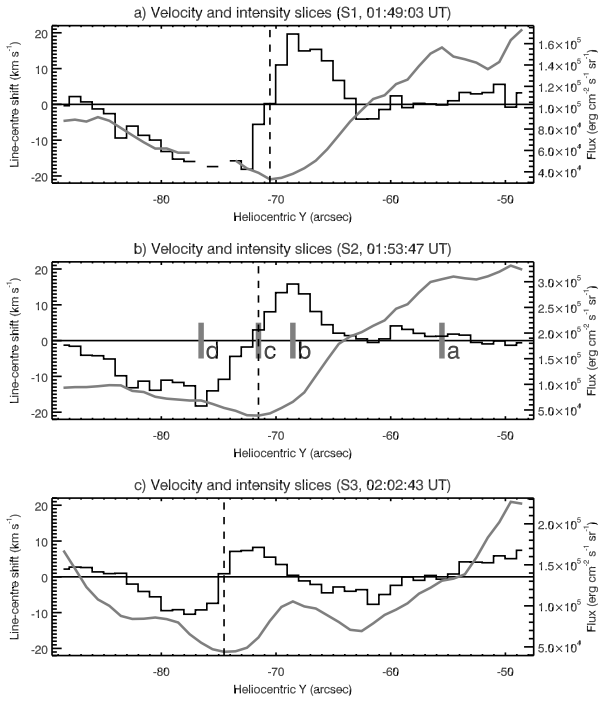

Fig. 2. Velocity and intensity slices along lines S1 to S3 in Figure 1. Black stepped lines indicate fitted line-centre shift in km s^{-1} (left vertical scale), while solid grey lines indicates the intensity along the same slices. The zero-velocity line is marked with a solid horizontal line. Vertical dashed lines indicate the position where the intensity minimum occurs along that slice, while labelled grey solid vertical lines correspond to the positions at which the profiles in Figure 3 are taken. Note the close correspondence between the intensity minimum and the point where the line centre shift is zero between opposing sides. Missing data points indicate poor fits to the model described in Section 2.2

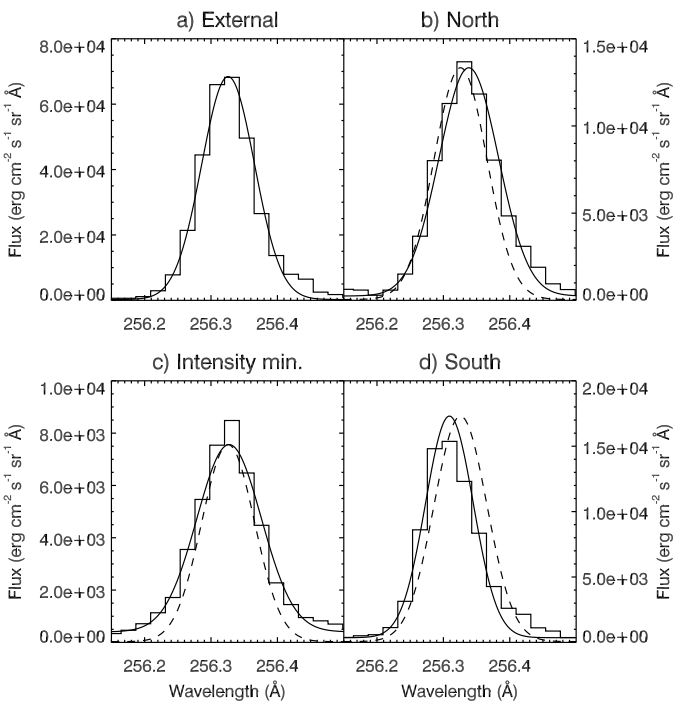

Fig. 3. EIS He II spectra (solid stepped lines) and single–Gaussian fitted line profiles (smooth solid curves) at the four labelled points along slice S2 (Figure 1): a) The region outside the filament (for reference); b) the northern side of the filament, exhibiting redshifted emission; c) the darkest portion of the filament; d) the southern edge, exhibiting blueshifted emission. The dashed curve in panels b) through c) represents the scaled fit to the data in panel a), in order to illustrate the Doppler shifts with respect to the spectrum in panel (a). The instrumental width of around 0.06 Å has not been removed from the spectra shown here.

sion from a thin layer nearest the observer, perhaps in the so-called prominence-corona transition region (PCTR; Chiuderi & Drago 1991) where n_e is measured to be of order 10^{10} cm^{-3}, using O IV line ratios ($\log T \approx 5.2$; Madjarska et al. 2001).

The opacity discussed above has implications for the value of Doppler shifts obtained by fitting, since a number of radiative transfer effects will tend to broaden the line profile and move its centroid back toward the rest wavelength. As a result, the Doppler shift we measure by fitting the line profile is likely to be an underestimate of the true velocity. Nevertheless, we still detect in the unfitted data major excursions of an almost Gaussian line shape from the rest wavelength determined in Section 2.2 (Figure 3), rather than a simple broadening or splitting of the line as might be expected from an optically thin, or unresolved, rotating structure (Williams 2004).

The coherent region of red Doppler shift north of the filament axis in Figure 1c appears to be well matched in heliocentric x (and therefore in time) by the blue-shifted region to the south of the structure. Both areas are large – much larger than the point-spread function of EIS (2.7 arcsec corresponds to 68% encircled energy at this wavelength) – and so are unlikely to be due to statistical fluctuations caused by poor signal-to-noise, etc. He II λ256 is a strong emission line throughout the solar disc, so this is unlikely to be a concern: even along the darker filament core, the signal-to-noise in these observations is better than 100.

Taking the example slices $S1$ to $S3$ shown in Figure 2, we see that these Doppler shifts appear to be approximately antisymmetric about the filament axis, with magnitudes up to ≈20 km s^{-1}. This effect suggests rotation of the structure about its axis, similar to the effect noted by Schmieder et al. (2000) in He I 10830 Å. Indeed, there appears to be a close correspondence between negligible velocity along the line of sight and the intensity minimum of each slice, which we take to be the location of the filament axis. This is seen qualitatively in Figures 1c and 1d, but more quantitatively in Figure 2. We note that no such antisymmetric Doppler shift profiles are seen near the filament in the coronal Fe XII line at 195.12 Å. This indicates that the process responsible for the opposing Doppler shifts is effectively confined to plasma that is cooler than the peak formation temperature of Fe XII ($T = 1.6$ MK).

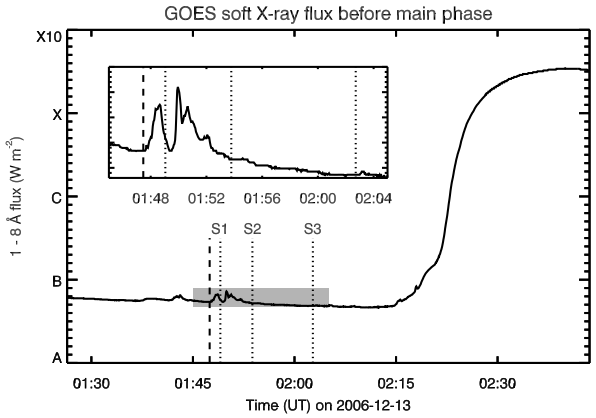

Fig. 4. GOES soft X-ray flux during the pre-flare and impulsive phases of the large eruption on 2006-12-13. (The flux in this band peaks at 02:14 UT.) The inset shows a magnification of the range shown by the grey shaded area. The dotted vertical lines indicate the times at which the corresponding slices in Figures 1 and 2 are made. The dashed vertical line indicates the first time at which an appreciable antisymmetric Doppler shift is seen across the filament axis (the westernmost crosses in Figures 1c and 1d). The last time it is noticeable coincides with the time of slice S3.

In Figure 4, we plot the soft X-ray flux in the 1–8 Å channel observed by the GOES satellites corresponding to the time leading up to, and including, the peak flare emission. It can be seen that the opposing Doppler shifts are visible just before a set of spikes in the pre-flare activity at around 01:48 UT. These spikes are present for less than half the duration of the opposing Doppler shifts' detectability (the latter lasting for 12 minutes).

3.2. Interpretation

We propose that the apparent rotation of the filament indicates that the initial equilibrium holding the filament in place is disturbed by some change in the surrounding magnetic environment. This may be due to small-scale flux emergence (Moore & Roumeliotis 1992), or it may be some form of so-called break-out (Antiochos et al. 1999; Aulanier et al. 2000). Either might be consistent with the low-level spikes in the solar soft X-ray flux seen at around the time as the oppositely directed flows are detected by EIS (Figure 4). It may be the case that they are continuations of the earlier small spikes in soft X-ray flux visible before 01:45 UT, with each successive spike indicating a liberation of the expanding structure.

Alternatively, the X-ray flux enhancements highlighted in the grey box of Figure 4 may be a reaction to the expansion of the filament, which in turn drives reconnection as current sheets are generated above and below the expanding structure (Török & Kliem 2005). In other words, we might interpret the lesser enhancements in SXR emission (before 01:45 UT) as indications of a causal reconnection (such as removal of tethers), whereas the SXR spikes highlighted in grey would be consequences of the current sheets formed by the flux rope's expansion.

For the case of an expanding flux rope which is initially line-tied to the photosphere, any given part of the expanding flux rope will be seen to rotate either towards or away from the observer, as the kink converts into writhe (Green et al. 2007) since the number of turns along a flux rope is assumed to remain constant. In the case of the ideal helical kink instability, this is illustrated in Figure 1 of Török & Kliem (2005)

The nature and apparent magnitude of the apparent anti-symmetric motions that we observe is similar to that seen in the resonance lines of C IV and Si IV in both quiet and active-region filaments by Engvold et al. (1985). However, since we almost certainly underestimate the true velocity by our observations, it may not be helpful to compare with these results quantitatively. Nonetheless, as Engvold et al. (1985) point out, oppositely directed motions on either side of the filament axis may be a natural consequence of flows that follow the magnetic field of either a 3-D generalised Kippenhahn & Schlüter (1957) model or a helical flux rope. This may be significant since flows are well observed along the axis of active region filaments (Tandberg-Hanssen 1974).

In this context, the timing and location of the observed antisymmetric motions that we present are of particular interest. Although EIS does not image the whole filament area at once, the oppositely directed motions we present are only detected in a narrow time range (13 min 40 s) significantly before the signatures of flare activity in GOES soft X-ray flux. This corresponds to a short section of the much larger filament, visible in He II intensity in Figure 1, over which such motions are not seen. In the cases presented by Engvold et al. (1985), the observations indicate that Doppler shifts are seen along most of the filaments analysed, rather than a smaller fraction as we detect here.

4. Conclusions

We present unparallelled EUV spectroscopic observations of an active region filament before a major solar flare in the He II λ256.32 line, one of the strongest emission lines observed by *Hinode*/EIS. The superior velocity resolution of this instrument allows us to detect large, coherent patches of opposing Doppler shifts, antisymmetric about the filament axis, and extending at least 30″ (22 Mm) along the filament axis.

We interpret these shifts as indications that at least part of the structure undergoes some rotation for a minimum of twelve minutes, ending more than ten minutes before the initial rise phase of the flare. Furthermore, the start of this apparent rotation immediately precedes a bursty enhancement in solar GOES SXR flux. Combining these details, we suggest that the filament is destabilised by a localised reorganisation of the magnetic field and rises, thereby expanding along its axis – that is, the flux rope bearing the filament rises in its centre, but with its footpoints still 'attached' to the photosphere – in a manner consistent with the early phase of the simulations of the helical-kink (Török & Kliem 2005) or torus (Török & Kliem 2007) instabilities; we suggest that the associated internal motions of the field lines in

the flux rope lead to the observed antisymmetric bulk velocities. We leave discussion of the details of this flyx rope expansion to future work, but point to recent modelling of instabilities thought to be responsible for the acceleration of flux ropes into coronal mass ejection material.

Hinode is a Japanese mission developed and launched by ISAS/JAXA, with NAOJ as domestic partner and NASA and STFC (UK) as international partners. It is operated by these agencies in co-operation with ESA and NSC (Norway). DRW acknowledges support from the UK Science and Technology Facilities Council (formerly PPARC). DHB acknowledges support from the NASA Hinode programme. The authors thank the referee for helpful comments towards presenting the results herein.

References

Amari, T., & Luciani, J. F., 1999, ApJL, 515, L81
Amari, T., Luciani, J. F., Mikic, Z., & Linker, J., 1999, ApJL, 518, L57
Antiochos, S. K., Devore, C. R., & Klimchuk, J. A., 1999, ApJ, 510, 485
Aulanier, G., DeLuca, E. E., Antiochos, S. K., McMullen, R. A., & Golub, L., 2000, ApJ, 540, 1126
Chen, P. F., & Shibata, K., 2000, ApJ, 545, 524
Chiuderi, C., & Drago, F. C., 1991, Sol. Phys., 132, 81
Culhane, J. L., Bone, L., Williams, D. R., Brooks, D. H., Vandriel-Gesztelyi, L., Hara, H., & Veronig, A., 2007, American Geophysical Union, 52, 05
Engvold, O., Tandberg-Hanssen, E., & Reichmann, E., 1985, Sol. Phys., 96, 35
Freeland, S. L., & Handy, B. N., 1998, Sol. Phys., 182, 497
Green, L. M., Kliem, B., Török, T., van Driel-Gesztelyi, L., & Attrill, G. D. R., 2007, Sol. Phys., 246, 365
Handy, B. N., et al., 1999, Sol. Phys., 187, 229
Jordan, C., 1967, Sol. Phys., 2, 441
Kippenhahn, R., & Schlüter, A., 1957, Zeitschrift fur Astrophysik, 43, 36
Kosugi, T., et al., 2007, Sol. Phys., 243, 3
Madjarska, M. S., Vial, J.-C., Bocchiallini, K., & Dermendjiev, V. N., 2001, in Recent Insights into the Physics of the Sun and Heliosphere: Highlights from SOHO and Other Space Missions, IAU Symposium, volume 203, eds. P. Brekke, B. Fleck, & J. B. Gurman, IAU Symposium, volume 203, 410
Moore, R. L., & Roumeliotis, G., 1992, Eruptive Solar Flares. Proceedings of Colloquium #133 of the International Astronomical Union, 399, 69
Rust, D. M., & Kumar, A., 1994, Sol. Phys., 155, 69
Schmieder, B., Delannée, C., Yong, D. Y., Vial, J. C., & Madjarska, M., 2000, A&A, 358, 728
Tandberg-Hanssen, E., 1974, Geophysics and Astrophysics Monographs, 12
Török, T., & Kliem, B., 2005, ApJ, 630, L97
Török, T., & Kliem, B., 2007, Astronomische Nachrichten, 328, 743
Williams, D. R., 2004, Proceedings of 'SOHO 13 - Waves, 547, 513
Williams, D. R., Török, T., Démoulin, P., van Driel-Gesztelyi, L., & Kliem, B., 2005, ApJ, 628, L163